Ripples in a string coupled to Glauber spins

L. L. Bonilla, A. Carpio, A. Prados, and R. R. Rosales

Phys. Rev. E **85**, 031125 — Published 19 March 2012

DOI: 10.1103/PhysRevE.85.031125

Ripples in a string coupled to Glauber spins

L L Bonilla[1], A Carpio[2], A Prados[3], R R Rosales[4]
[1] *G. Millán Institute for Fluid Dynamics, Nanoscience and Industrial Mathematics, Universidad Carlos III de Madrid, 28911 Leganés, Spain*
[2] *Departamento de Matemática Aplicada, Universidad Complutense de Madrid, 28040 Madrid, Spain*
[3] *Física Teórica, Universidad de Sevilla, Apartado de Correos 1065, E-41080, Sevilla, Spain and*
[4] *Dept. of Mathematics, Massachusetts Inst. of Technology, 77 Massachusetts Avenue, Cambridge, MA 02139, USA*

Each oscillator in a linear chain (a string) interacts with a local Ising spin in contact with a thermal bath. These spins evolve according to Glauber dynamics. Below a critical temperature, there appears an equilibrium, time-independent, rippled state in the string that is accompanied by a nonzero spin polarization. On the other hand, the system is shown to form "metastable", nonequilibrium but long-lived ripples in the string for slow spin relaxation. The system vibrates rapidly about these quasi-stationary states which can be described as snapshots of a coarse-grained stroboscopic map. For moderate observation times, ripples are observed irrespective of the final thermodynamically stable state (rippled or not). Interestingly, the system can be considered as a "minimal" model to understand rippling in clamped graphene sheets.

PACS numbers: 05.40.-a; 64.60.De; 05.45.-a

I. INTRODUCTION

Mechanical systems coupled to spins are used to describe structural phase transitions. Examples include the collective Jahn-Teller effect [1], structural phase transitions with a scalar order parameter exhibiting a central peak in the dynamic response function [2] and criticality in martensites and externally driven models [3]. In many of these models, the mechanical system provides a long range interaction between the spins that produces a phase transition in which the spin polarization ceases to be zero below a critical temperature. While most studies consider the effective spin system obtained after eliminating the mechanical degrees of freedom, it is interesting to focus instead on the effect of the phase transition on the mechanical system. In this paper, we consider mechanical systems coupled to Ising spins that undergo Glauber dynamics [4] in contact with a thermal bath (a single harmonic oscillator connected to Ising spins in the simplest case [5]). There is a phase transition at a critical temperature below which the spin polarization is nonzero and ripples appear in the mechanical system. These thermodynamically stable ripples are inhomogeneous stationary states of the mechanical system, which are quite simple below the critical temperature. On the other hand, there are long-lived dynamical ripples with a wide variety of shapes at any temperature provided the period of mechanical vibrations is short compared to the spin relaxation time. In this limit, the spins are frozen during long time intervals between spin flips and they fix a quasi-stationary state about which the mechanical system oscillates. Observations of the system may consist of time averages over intervals sufficiently long to include many oscillation periods but short compared to the intervals between spin flips. Then these observations will sample a coarse-grained stroboscopic map consisting of successive quasi-stationary states that show ripples. After a much longer time during which sufficiently many spin flips have occurred and due to the dissipation introduced by the Glauber spin dynamics, the ripples eventually evolve to the simple version obtained from the equilibrium thermodynamics of the spin-mechanical system.

These considerations may apply to the evolution of ripples in suspended graphene sheets. Ripples are undulations of the sheet with characteristic amplitudes and wave lengths that, according to experiments, do not have a preferred direction [6]. Time resolved ripples and defects in graphene sheets can be observed using aberration corrected TEMs that collect data every other second, a time much longer than microscopic times such as the one it takes a sound wave to cross one lattice constant [7]. As a direct generalization of theories of defect motion in planar graphene [8], atom motion in a suspended graphene sheet may be described by the von Karman equations discretized on a hexagonal lattice [9]. Coupling the vertical motion of graphene atoms with an Ising spin located at the same lattice point may account for a spontaneous trend of the sheet to bend upwards or downwards. Spin dynamics adds dissipation to the von Karman equations and thus the spin relaxation time should be much longer than microscopic mechanical times. Experimental observations are taken over long time intervals and therefore should correspond to different takes of a coarse-grained stroboscopic map similar to that described in this paper.

The plan of the paper is as follows. In Section II, we introduce the model and study the rippling phase transition which appears therein. Section III is devoted to the analysis of the slow spin relaxation regime. In this limit, we will see that meastable long-lived ripples appear, which are different from the "static" ripples found in sec. II. We present arguments that support that these metastable ripples are the relevant ones, in connection with the rippling of graphene sheets. The continuum limit of the model, together with the opposite limit of

fast spin relaxation, is investigated in Section IV. Finally, we present the main conclusions of the paper in section V.

II. MODEL AND RIPPLING PHASE TRANSITION

Our mechanical system is a chain of oscillators with next-neighbor interaction which becomes a string in the continuum limit:

$$\mathcal{H} = \sum_{j=0}^{N} \left[\frac{p_j^2}{2m} + \frac{m\omega^2}{2}(u_{j+1} - u_j)^2 - f u_j \sigma_j \right], \qquad (1)$$

with $u_0 = 0 = u_{N+1}$. The jth oscillator is coupled linearly to an Ising spin $\sigma_j = \pm 1$. The spins are in contact with a thermal bath at temperature T and flip stochastically following Glauber's dynamics [4] at temperature T. Unlike the case of a regular mass-springs chain, here each triplet is biased against being straight, with $u_{j+1} - u_j = u_j - u_{j-1}$. The applied force (whose sign flips at random) makes the "preferred" state at any instant a wedge shape. This translates the loose idea that the three carbon links each atom shares to build the graphene sheet do not want to be in a plane because of the fourth "free" link (which may push the atoms up or down the horizontal planar configuration). The free chemical bonds of the carbon lattice in the graphene sheet may be assimilated to our spins, which interact with phonons modeled by the oscillators. Of course, in order to have a more realistic model of a clamped graphene sheet, the structure of its 2D lattice should be taken into account. Nevertheless, we hope that this simple model will be able to capture the main physical mechanism involved in the rippling of graphene sheets. In our model, we have chosen boundary conditions (bc) corresponding to a suspended graphene sheet that is clamped at its edges. We can consider different bc, corresponding to other physical situations, but the bc do not affect the physical mechanism giving rise to ripple formation. For the sake of brevity, we will only consider the clamped case throughout this paper.

Thus at any time t, the system may experience a transition from $(\mathbf{u}, \mathbf{p}, \sigma)$ to $(\mathbf{u}, \mathbf{p}, R_j\sigma)$ at a rate given by [4]

$$W_j(\sigma|\mathbf{u}, \mathbf{p}) = \frac{\alpha}{2}\left(1 - \beta_j \sigma_j\right), \quad \beta_j = \tanh\left(\frac{f u_j}{k_B T}\right), \quad (2)$$

where $R_j\sigma$ is the configuration obtained from σ by flipping the j-th spin and k_B is the Boltzmann constant. The parameter α gives the characteristic attempt rate for the transitions in the Ising system. Individual spins experience a mutual long-range interaction through their coupling to the string. This long-range interaction causes a phase transition of the spin system: the spins have nonzero polarization for $T < T_c$ whose counterpart for the string is the formation of ripples. To see this, we find the following effective potential by integrating $e^{-\mathcal{H}/(k_B T)}$ over the spin configurations [5], with the result:

$$\mathcal{V}_{\text{eff}} = \sum_{j=0}^{N} \left[\frac{1}{2} m\omega^2 (u_{j+1} - u_j)^2 - k_B T \ln\cosh\left(\frac{f u_j}{k_B T}\right) \right]. \qquad (3)$$

The extrema of this potential satisfy

$$m\omega^2(u_{j+1} + u_{j-1} - 2u_j) + f \tanh\left(\frac{f u_j}{k_B T}\right) = 0. \qquad (4)$$

Let us analyze the stability of the trivial solution $u_j = 0$ (horizontal string, no ripples). We look for solutions $U_j = e^{ijk}$ of the linearization of eq. (4),

$$U_{j+1} + U_{j-1} - 2U_j + \frac{f^2 U_j}{m\omega^2 k_B T} = 0, \quad j = 1, \ldots, N, \quad (5)$$

with clamped bc $U_0 = U_{N+1} = 0$. The condition $U_0 = 0$ implies that we only have to consider the imaginary part, $U_j = \sin(jk)$, whereas $U_{N+1} = 0$ restricts the possible values of k, so that only $k_n = n\pi/(N+1)$, $n = 1, \ldots, N+1$, are possible. Finally, if U_j solves eq. (5), the wave number k must be related to the temperature through $f^2/(m\omega^2 k_B T_n) = 4\sin^2(k_n/2)$. This expression defines a set of critical temperatures T_n, at which rippled solutions, characterized by a wave number k_n, of Eq. (5) emerge. The largest possible critical temperature corresponds to $n = 1$,

$$T_c \equiv T_1 = \frac{f^2 K_N^2}{k_B m\omega^2}, \quad K_N = [2\sin(k_1/2)]^{-1} \sim \frac{N}{\pi}, \quad (6)$$

in the large system size limit $N \gg 1$.

The dependance of this critical temperature with the system size N hinges on how the model parameters m, ω, f scale with N. Of course, these scalings depend on the details of the microscopic model which, in some limit, can be described by the stochastic dynamics we have introduced. We assume that the frequency $\omega \propto N$, while m and f are independent of the system size. In Section IV of the paper, we will show that this scaling implies that both the effective potential (3) and the nonlinear equation (4) have a well-defined continuum limit [10]. This is a sensible property, since graphene sheets are often and successfully modeled by means of continuum elasticity [11–15]. Thus we define $\omega_0 = \omega/K_N$, which is of the order of unity in the large system size limit as $N \gg 1$. Then the critical temperature T_c remains finite as $N \to \infty$,

$$T_c = \frac{f^2}{m\omega_0^2 k_B}, \qquad \omega_0 \equiv \frac{\omega}{K_N}. \qquad (7)$$

Let us briefly consider other possible scalings of the hamiltonian parameters with the system size. For other scalings, the expression (7) for the critical temperature T_c remains valid, but ω_0 is no longer of order 1. For instance, if all the parameters in the hamiltonian (1) are independent of the system size, T_c diverges in the large

system size limit $N \gg 1$. This means that the flat configuration of the string becomes unstable for all temperatures in this limit. Nevertheless, for any finite value of N, there should be an "effective" critical temperature T_c, above which the flat configuration would be stable.

In the following, we will restrict ourselves to the case $\omega_0 = \mathcal{O}(1)$, independent of the system size. There is a well-defined phase transition at $T = T_c$, then we define a dimensionless temperature $\theta = T/T_c$. For $T > T_c$ ($\theta > 1$) the trivial solution of (4) is linearly stable and for $T < T_c$ ($\theta < 1$) it is unstable and there appear stable non-uniform states corresponding to static ripples in the string. Using nondimensional variables $u_j^* = fu_j/(k_B T_c) = m\omega_0^2 u_j/f$ and omitting the asterisks so as not to clutter the formulas, the first such state is proportional to the sinusoidal mode with k_1

$$u_j = \pm 2\sqrt{1-\theta}\,\sin\left(\frac{\pi j}{N+1}\right) + O(|1-\theta|), \tag{8}$$

in the limit as the reduced temperature θ tends to 1 from below. Equation (8) is derived in Appendix A, making use of bifurcation theory. According to Appendix A, initial conditions that are not orthogonal to $\sin[j\pi/(N+1)]$ decay to (8) as $e^{-\delta t/2}$ for $\delta = \alpha/\omega_0 < 2$ and $\theta \sim 1$. At the lower critical temperatures $\theta_n = \sin^2 k_1/\sin^2 k_n < 1$, $n > 1$, other non-uniform states proportional to the sinusoidal modes with $k = k_n$ ($n-1$ interior nodes) bifurcate from the trivial solution. These non-uniform solutions have a nonzero spin polarization $\langle \sigma_j \rangle \sim \tanh(fu_j/(k_B T_n))$ and therefore the critical temperatures θ_n are associated with cooperative Jahn-Teller phase transitions, in which coupling to phonons (the string) breaks the symmetry of a doubly degenerated electronic state (the spins) [1]. Numerical simulations of the spin-string system confirm this. Below T_c, stable string configurations are stationary, nonuniform and exhibit ripples. To test the bifurcation theory, we have performed stochastic simulations at temperatures $\theta > 1$ and $\theta = 0.9$ for $\delta = 0.1$ and $N = 10^4$. In Figure 1, we show how an initially flat string at rest evolves to a state close to (8). The initial conditions are random spins, such that the average spin polarization has a sinusoidal shape, and a horizontal, zero-velocity string profile. A qualitatively analogous behavior is found for the majority of initial spin configurations, but for some of them the unstable flat string configuration is stabilized (see Appendix A). This is a stabilization of the thermodynamically unstable state akin to the one previously found for a single oscillator coupled to Glauber spins [5]. For lower temperatures a similar stationary state without internal nodes is stable whereas the stationary states with $n-1$ internal nodes that bifurcate from the flat string configuration at temperatures T_n are unstable.

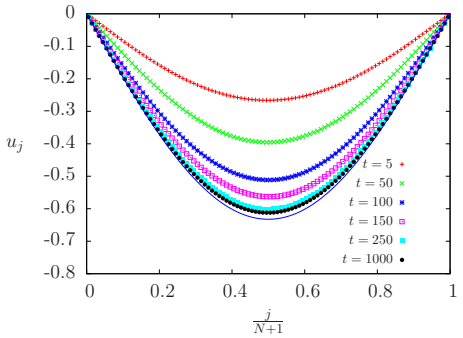

FIG. 1: (Color online) Stable ripple state without internal nodes for $\theta = 0.9$, $\delta = \alpha/\omega_0 = 0.1$ and $N = 10^4$. For each trajectory, the initial configuration consists of a flat string at rest and random spins, such that the average spin polarization has a sinusoidal shape. Averages over 100 trajectories and spatial averages over 100 oscillators centered at a given one have been performed in order to ensure good averages. See also movie in the Supplemental Material [17].

III. SLOW SPIN RELAXATION

Additional insight can be obtained in the limit $\delta = \alpha/\omega_0 \ll 1$, in which the spin flip rate is slow compared to the characteristic string frequency. In the following, we will use a dimensionless time $t^* = \omega_0 t$, and omit the asterisks as before. Then the u_j's obey the equation of motion

$$\ddot{u}_j - K_N^2(u_{j+1} + u_{j-1} - 2u_j) = \sigma_j, \tag{9}$$

for $j = 1, \ldots, N$ with boundary conditions $u_0 = u_{N+1} = 0$ ($\ddot{u} = d^2u/dt^2$). The spins σ_j are stochastic variables which flip at a rate $W_j(\sigma|\mathbf{u},\mathbf{p}) = \delta(1-\beta_j\sigma_j)/2$, $\beta_j = \tanh(u_j/\theta)$, $\theta = T/T_c$ instead of (2). Let us consider a trajectory of the system, for given initial states of the string and spins. Since the spin flip rate is very small, the spins are frozen at fixed values during time intervals that are long compared to the longest oscillation period of the string. During the time interval before the spin flip occurs, we may split the solution of (9) in a quasi-stationary and a time-dependent part according to (see Appendix B):

$$u_j(t) = u_j^s + v_j(t), \tag{10}$$

$$u_j^s = \frac{1}{K_N^2}\left[j\sum_{l=1}^{N}\left(1 - \frac{l}{N+1}\right)\sigma_l - \sum_{l=1}^{j-1}(j-l)\sigma_l\right], \tag{11}$$

$$v_j(t) = \sum_{n=1}^{N}[A_n\cos(\Omega_n t) + B_n\sin(\Omega_n t)]\phi_{n,j}, \tag{12}$$

where

$$\Omega_n = 2K_N\sin\left(\frac{\pi n}{2(N+1)}\right), \tag{13}$$

$$\phi_{n,j} = \sqrt{\frac{2}{N+1}}\sin\left(\frac{\pi n j}{N+1}\right), \tag{14}$$

$$A_n = \sum_{j=1}^{N}[u_j(0) - u_j^s]\phi_{n,j},\ B_n = \sum_{j=1}^{N}\dot{u}_j(0)\phi_{n,j}. \tag{15}$$

The string profiles in (10) represent vibrations of the string about the quasi-stationary configuration in (11) whose longest period is 2π ($\Omega_1 = 1$ is the lowest frequency). Now let the first spin that flips after $t = 0$ be σ_{j_1}, which changes sign at time t_1. Immediately after t_1, the right hand side (RHS) of (9) should be replaced by $\sigma_j - 2\delta_{j_1 j}\sigma_{j_1}\Theta(t-t_1)$, where $\Theta(x) = 1$ for $x \geq 0$, $\Theta(x) = 0$ for $x < 0$ is the unit step function. The changes in u_j^s and $v_j(t)$ due to the spin flip at t_1 are

$$\Delta u_j^s = \frac{2\sigma_{j_1}}{K_N^2}\left[\Theta(j-j_1-1)(j-j_1) - j\left(1-\frac{j_1}{N+1}\right)\right], \quad (16)$$

$$\Delta v_j = -\sum_{n=1}^{N}\left(\sum_{l=1}^{N}\Delta u_l^s \phi_{n,l}\right)\phi_{n,j}\cos[\Omega_n(t-t_1)], \quad (17)$$

respectively, for $t > t_1$. Successive spin flips produce changes similar to (16) and (17) in the quasi-stationary and time-dependent parts of $u_j(t)$, respectively, at times $t_2, t_3, \ldots$ with $t_l - t_{l-1} = O((N\delta)^{-1})$. Time averages over sufficiently long time intervals that are short compared to $(N\delta)^{-1}$ eliminate $v_j(t)$. Thus successive snapshots of averaged string profiles coincide with updated quasi-stationary u_j^s profiles. The latter constitute a coarse-grained stroboscopic map showing how the ripples in the string evolve to their final stable configurations: the horizontal string for $\theta > 1$ or a simple parabolic-like profile above or below the horizontal string for $\theta < 1$. Figure 2 depicts snapshots of the coarse-grained stroboscopic map for an initially flat string at rest with (a) a spin configuration exhibiting seven domains and (b) completely random spins for a temperature $\theta = 0.1$, below the critical one. For moderate time intervals stable ripples are observed whereas the stationary configuration of the string without internal nodes is reached at extremely long time intervals. Rippling behavior is also observed for above critical temperatures, $\theta > 1$, but the string eventually approaches the flat configuration. In time-resolved experiments such as those with suspended graphene sheets [7], data are taken in long time intervals (1 second), which we use as an estimate for the spin flip attempt rate α. Typical times ω_0^{-1} are 1 ps, therefore $\delta \simeq 10^{-12}$ and the number of spins per linear dimension $N \simeq 10^4$ for square 1 micron samples. Thus, $1/(N\delta) \approx 10^8$ (much larger than the value considered in Fig. 2) and ripple states corresponding to snapshots of the coarse-grained stroboscopic map are observed. The "true" thermodynamically stable state would only be reached for extremely long time intervals, much longer than the total observation time in an experiment. On a physical basis, one may expect that the characteristic time associated to the spin flips in graphene be larger than the data-collecting time (1 s), so our estimate for the time between spin flips is actually a lower bound to the actual value. The movie in the Supplemental Material illustrates how the string vibrates rapidly about the quasi-stationary configurations corresponding to successive snapshots of the coarse-grained stroboscopic map [17]. Given the large separation between microscopic times, data collection times and duration of a given experiment, it is important to remark that *ripples are observed for all current time-resolved experiments no matter what the temperature and the thermodynamically stable state are. Thus ripples are inherently dynamical and explanations based on thermodynamically stable states do not capture the essence of rippling.*

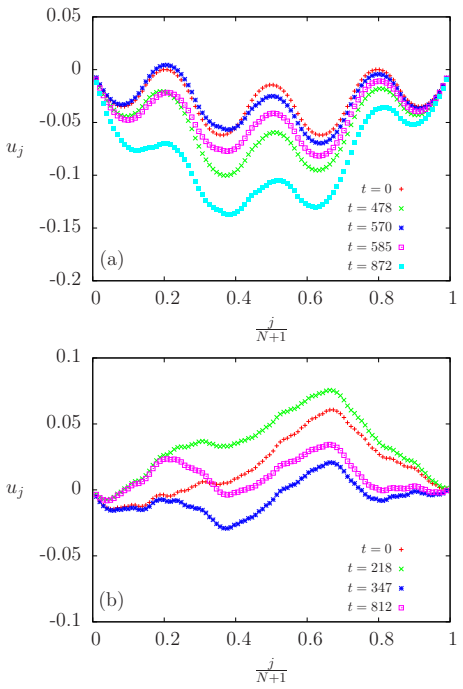

FIG. 2: (Color online) Four snapshots of the coarse-grained stroboscopic map for $\theta = 0.1$, $\delta = 10^{-4}$ and $N = 100$ up to $t = 10^3$. The initial configuration consists of a flat string at rest and the spins are (a) initially distributed in seven spin domains of alternating sign or (b) randomly distributed. The times corresponding to the spin flips which change the quasi-stationary string profile are indicated. Ripples with several domains persist for long times whereas the stable configuration corresponding to a string without internal nodes is reached in a much longer time larger than 10^4. See also movie in the Supplemental Material illustrating how the string oscillates about quasi-stationary configurations given by the coarse-grained stroboscopic map [17].

IV. CONTINUUM LIMIT AND FAST SPIN RELAXATION

Further analysis of string ripples can be done in the continuum limit $N \to \infty$. From (1) and (2), we obtain equations for the averages of u_j and σ_j. If we split the variables $u_j = \widetilde{u}_j + \Delta u_j$, where $\widetilde{u}_j = \langle u_j \rangle$, set $\widetilde{q}_j = \langle \sigma_j \rangle$ and ignore the fluctuations Δu_j in the limit $N \to \infty$, we get the following nondimensional *macroscopic equations*:

$$\ddot{\widetilde{u}}_j = K_N^2(\widetilde{u}_{j+1} + \widetilde{u}_{j-1} - 2\widetilde{u}_j) + \widetilde{q}_j, \quad (18)$$

$$\dot{\widetilde{q}}_j = \delta\left[\tanh\left(\frac{\widetilde{u}_j}{\theta}\right) - \widetilde{q}_j\right], \quad (19)$$

for $j = 1, \ldots, N$. We now set $\tilde{u}_j(t) = \tilde{u}(x,t)$ with $x = j/K_N$ and take the continuum limit. Then (18)-(19) become

$$\frac{\partial^2 \tilde{u}}{\partial t^2} - \frac{\partial^2 \tilde{u}}{\partial x^2} = \tilde{q}, \quad \frac{\partial \tilde{q}}{\partial t} + \delta \tilde{q} = \delta \, \tanh\left(\frac{\tilde{u}}{\theta}\right), \tag{20}$$

to be solved with the boundary conditions $\tilde{u}(0,t) = \tilde{u}(\pi,t) = 0$. In the limit $\delta \gg 1$ (fast relaxation of the spins compared to the string time scale), we can approximate the second equation in (20) by $\tilde{q} \approx \tanh(\tilde{u}/\theta) + [\delta\theta \cosh^2(\tilde{u}/\theta)]^{-1} \partial\tilde{u}/\partial t$ and insert this in the first equation. The result is

$$\frac{\partial^2 \tilde{u}}{\partial t^2} + \frac{1}{\delta\theta \cosh^2\left(\frac{\tilde{u}}{\theta}\right)} \frac{\partial \tilde{u}}{\partial t} - \frac{\partial^2 \tilde{u}}{\partial x^2} = \tanh\left(\frac{\tilde{u}}{\theta}\right), \tag{21}$$

whose stationary solutions satisfy the equation

$$\frac{d^2 \tilde{u}}{dx^2} + \tanh\left(\frac{\tilde{u}}{\theta}\right) = 0, \tag{22}$$

which is the continuum limit of eq. (4). A stability analysis of the flat solution $\tilde{u}(x) = 0$ can be done along the same lines of the study of its discrete version (4). The result is that the flat solution $\tilde{u}(x) = 0$ is stable for $\theta > 1$, while

$$\tilde{u}(x) = \pm 2\sqrt{1-\theta}\, \sin x + O(|1-\theta|), \tag{23}$$

is the stable string state just below $\theta = 1$. Of course, eq. (23) is the continuum limit of the discrete expression (8). Moreover, this solution can be rederived by analyzing the minima of the continuum limit of the effective potential (3),

$$\mathcal{V}_{\text{eff}} \sim \frac{N k_B T_c}{\pi} \int_0^\pi dx \left[\frac{1}{2}\left(\frac{\partial u}{\partial x}\right)^2 - \theta \ln \cosh\left(\frac{u}{\theta}\right)\right], \tag{24}$$

where u is written in the same nondimensional units as $\tilde{u}$. The condition for a profile to be a extremum of the effective potential is nothing but the nonlinear equation (22) . The small damping term in (21) stabilizes the flat solution $u(x) = 0$ above the critical temperature and the stationary ripple solutions below it. The consistency of the scaling introduced in section II must be stressed: in the continuum limit, the effective potential is an extensive quantity, proportional to the system size N.

The opposite limit of $\delta \ll 1$ has already been studied using the coarse-grained stroboscopic map. It is interesting to note that we obtain a nonlinear Duffing equation from a two-term expansion of the hyperbolic functions in (21). Similar nonlinear equations have been recently proposed to model graphene resonators on a phenomenological basis.[11, 16]

V. CONCLUSIONS

We have shown that stable ripples appear in a 1D string when each oscillator is coupled to an Ising spin and the latter are in contact with a thermal bath at temperature T. Below a critical temperature, the thermodynamically stable string profile is not flat, but nonuniform without internal nodes. In spite of the simplicity of the thermodynamically stable state, more complex ripples appear when the spin flip rate is much smaller than the oscillator period. Although strictly speaking these ripples are evolving in time, they are very long-lived metastable states. The ripples are snapshots of a coarse-grained stroboscopic map depicting the average of the rapid string motion over long time intervals. Whether the final thermodynamically stable is the flat or bent string, ripples should be observed on reasonable time intervals at any temperature.

The system considered here is far from being a realistic model of a graphene sheet. However, the free chemical bonds of the carbon lattice in the latter may be assimilated to our spins, which interact with the phonons modeled by the oscillators. Thus, 2D ripples analogous to the ones found here should appear. This opens the door to understanding the characteristic rippling shown by graphene sheets at any temperature as an inherently dynamical phenomenon, whose physical mechanism consists of the interaction between free bonds and phonons with widely separated time scales.

This research has been supported by the Spanish Ministerio de Economía y Competitividad through Grants FIS2011-28838-C02-01 (LLB), FIS2011-28838-C02-02 (AC), FIS2011-24460 (AP, partially financed by FEDER funds) and FIS2010-22438-E (Spanish National Network Physics of Out-of-Equilibrium Systems), by UCM/BSCH CM 910143 (AC) and by the National Science Foundation grant DMS-0907955 (RRR).

Appendix A: Bifurcation calculations

Let us consider the nondimensional macroscopic equations (18)-(19) of the paper:

$$\frac{d^2 u_j}{dt^2} = K_N^2 (u_{j+1} + u_{j-1} - 2u_j) + q_j, \tag{A1}$$

$$\frac{dq_j}{dt} = \delta \left[\tanh\left(\frac{u_j}{\theta}\right) - q_j\right], \tag{A2}$$

$j = 1, \ldots, N$, with $u_0 = 0$, $u_{N+1} = 0$. Here we omit the tildes for simplicity. Near the critical temperature $\theta = 1$, we make the Ansatz

$$u_j(t;\epsilon) = \epsilon \sum_{l=0}^{2} \epsilon^l u_j^{(l)}(t,s) + O(\epsilon^4), \tag{A3}$$

$$q_j(t;\epsilon) = \epsilon \sum_{l=0}^{2} \epsilon^l Q_j^{(l)}(t,s) + O(\epsilon^4), \tag{A4}$$

$$\theta = 1 - \epsilon^2 \theta_2, \quad s = \epsilon^2 t, \quad \tilde{t} = t, \tag{A5}$$

where ϵ is a small parameter measuring the amplitude of the bifurcating solution. Inserting these equations in

(A1) and (A2), we get the following hierarchy of equations:

$$\mathbb{L}u_j^{(0)} - q_j^{(0)} \equiv \frac{\partial^2 u_j^{(0)}}{\partial t^2} + K_N^2(2u_j^{(0)} - u_{j+1}^{(0)} - u_{j-1}^{(0)}) - q_j^{(0)} = 0, \quad \text{(A6)}$$

$$\mathbb{M}q_j^{(0)} - \delta u_j^{(0)} \equiv \frac{\partial q_j^{(0)}}{\partial t} + \delta q_j^{(0)} - \delta u_j^{(0)} = 0, \quad \text{(A7)}$$

$$\mathbb{L}u_j^{(1)} - q_j^{(1)} = 0, \quad \text{(A8)}$$

$$\mathbb{M}q_j^{(1)} - \delta u_j^{(1)} = 0, \quad \text{(A9)}$$

$$\mathbb{L}u_j^{(2)} - q_j^{(2)} = -2\frac{\partial^2 u_j^{(0)}}{\partial t \partial s}, \quad \text{(A10)}$$

$$\mathbb{M}q_j^{(2)} - \delta u_j^{(2)} = \delta\left(\theta_2 u_j^{(0)} - \frac{1}{3}u_j^{(0)\,3}\right) - \frac{\partial q_j^{(0)}}{\partial s}, \quad \text{(A11)}$$

and so on.

At the critical temperature $\theta = 1$, the eigenvalues corresponding to the linear system (A6) - (A7) are 0 and $-\frac{\delta}{2} \pm i\sqrt{1-\delta^2/4}$ (for $\delta < 2$). Thus the solution of (A6) - (A7) is

$$u_j^{(0)} = A(s)\phi_{1,j} = q_j^{(0)}, \quad \text{(A12)}$$

$$\phi_{1,j} = \sqrt{\frac{2}{N+1}}\,\sin\left(\frac{\pi j}{N+1}\right),$$

where we have omitted terms that decrease exponentially as $e^{-\delta t/2}\cos[t\sqrt{1-\delta^2/4}+\gamma]$. Insertion of (A12) in (A10)-(A11) yields

$$\mathbb{L}u_j^{(2)} - q_j^{(2)} = 0, \quad \text{(A13)}$$

$$\mathbb{M}q_j^{(2)} - \delta u_j^{(2)} = \left(\delta\theta_2 A - \frac{dA}{ds} - \frac{\delta A^3}{3}\phi_{1,j}^2\right)\phi_{1,j}. \quad \text{(A14)}$$

The right hand side of (A14) should be orthogonal to the eigenvector $\phi_{1,j}$ for this system to have a solution bounded as $t \to \infty$. Using that $\sum_{j=1}^N \phi_{1,j}^2 = 1$ (see eq. (B10) of Appendix B) and

$$\left(\frac{2}{N+1}\right)^2 \sum_{j=1}^{N} \sin^4\left(\frac{\pi j}{N+1}\right) = \frac{3}{2(N+1)}, \quad \text{(A15)}$$

we obtain

$$\frac{dA}{ds} = \delta A\left(\theta_2 - \frac{A^2}{2(N+1)}\right), \quad \text{(A16)}$$

whose solution is

$$A(s) = \text{sign}[A(0)]\sqrt{\frac{2(N+1)\theta_2}{1 + e^{-2\theta_2\delta s}\left(\frac{2(N+1)\theta_2}{A(0)^2} - 1\right)}}. \quad \text{(A17)}$$

As $s \to \infty$, $A(s)$ vanishes for $\theta_2 = -1$ and it tends to $\pm\sqrt{2(N+1)}$ for $\theta = 1$. This is the typical behavior of a supercritical pitchfork bifurcation of stable non-uniform stationary spin and string profiles from the trivial solution. For $\theta < 1$, we obtain the corresponding profiles of the string and the spin systems by inserting (A17) in (A12) and (A3) and restoring $\theta = 1 - \epsilon^2\theta_2$ and the original time variable:

$$u_j = q_j = 2\,\text{sign}[A(0)]\sqrt{\frac{1-\theta}{1 + e^{-2\delta(1-\theta)t}\left(\frac{2(N+1)\theta_2}{A(0)^2} - 1\right)}} \times \sin\left(\frac{\pi j}{N+1}\right) + O(|1-\theta|), \quad \text{(A18)}$$

$$\epsilon A(0) = \sqrt{\frac{2}{N+1}}\sum_{j=1}^{N} q_j(0)\sin\left(\frac{\pi j}{N+1}\right). \quad \text{(A19)}$$

In (A18), we have ignored exponentially small terms proportional to $e^{-\delta t/2}$. Even when $\delta \ll 1$, these terms decay much faster than the exponential $e^{-2\delta(1-\theta)t}$ in (A18) as $(1-\theta) \to 0$. As $t \to \infty$, the stationary profiles vanish only at the end points of the string:

$$u_j = q_j = 2\,\text{sign}[A(0)]\sqrt{1-\theta}\,\sin\left(\frac{\pi j}{N+1}\right) + O(|1-\theta|). \quad \text{(A20)}$$

For $A(0) = 0$, the above equation should be understood as giving $u_j = q_j = 0$ for all j, because the solution of eq. (A16) with the initial condition $A(0)$=0 is $A(s) = 0$ for all s. Thus, the flat string configuration is stabilized for initial conditions such that $A(0) = 0$; for any other different condition the system eventually reaches one of the two symmetrical rippled profiles without internal nodes.

Similar calculations at the critical temperatures

$$T_n = \frac{f^2 K_N^2}{k_B m\omega^2\Omega_n^2}, \quad \Omega_n = \frac{\sin\left(\frac{\pi n}{2(N+1)}\right)}{\sin\left(\frac{\pi}{2(N+1)}\right)}, \quad \text{(A21)}$$

yield the following bifurcating stationary profiles

$$u_j = q_j = 2\,\text{sign}[A(0)]\frac{\sqrt{\theta_n - \theta}}{\Omega_n}\,\sin\left(\frac{\pi j n}{N+1}\right) + O(|\theta_n - \theta|), \quad \text{(A22)}$$

where $\theta_n = T_n/T_c$. In the continuum limit, (A22) becomes

$$u(x) = q(x) = \pm 2\frac{\sqrt{\theta_n - \theta}}{n}\,\sin(nx) + O(|\theta_n - \theta|), \quad \text{(A23)}$$

with $\theta_n = 1/n^2$, $n = 1, 2, \ldots$. The profiles (A23) vanish at $n-1$ interior points in $0 \le x \le \pi$.

Appendix B: Splitting of $u_j(t)$ in the limit $\alpha \ll \omega_0$

The stationary part u_j^s of $u_j(t)$ satisfies

$$-K_N^2(u_{j+1}+u_{j-1}-2u_j)=\sigma_j, \tag{B1}$$

for $j=1,\ldots,N$ according to Eq. (9) of the main text. Defining $w_j=u_{j+1}-u_j$, (B1) becomes

$$w_j-w_{j-1}=-\frac{\sigma_j}{K_N^2}, \tag{B2}$$

whose solution is

$$u_{j+1}-u_j=w_j=u_1-\frac{1}{K_N^2}\sum_{l=1}^{j}\sigma_l, \tag{B3}$$

because $w_0=u_1$ due to the boundary condition $u_0=0$. Summing (B3) from 1 to $j-1$, we find

$$u_j=ju_1-\frac{1}{K_N^2}\sum_{l=1}^{j-1}\sum_{k=1}^{l}\sigma_k. \tag{B4}$$

The other boundary condition $u_{N+1}=0$ yields

$$u_1=\frac{1}{(N+1)K_N^2}\sum_{l=1}^{N}\sum_{k=1}^{l}\sigma_k. \tag{B5}$$

These formulas can be simplified using summation by parts:

$$\begin{aligned}\sum_{l=1}^{j-1}\sum_{k=1}^{l}\sigma_k&=\sum_{l=1}^{j-1}[l-(l-1)]\sum_{k=1}^{l}\sigma_k?\\ &=\sum_{l=1}^{j-1}[l\sum_{k=1}^{l}\sigma_k-(l-1)\sum_{k=1}^{l-1}\sigma_k-(l-1)\sigma_l]\\ &=(j-1)\sum_{l=1}^{j-1}\sigma_l-\sum_{l=1}^{j-1}(l-1)\sigma_l=\sum_{l=1}^{j-1}(j-l)\sigma_l.\end{aligned} \tag{B6}$$

Substituting this in (B4) and (B5), we obtain

$$u_j=\frac{1}{K_N^2}\left[j\sum_{l=1}^{N}\left(1-\frac{l}{N+1}\right)\sigma_l-\sum_{l=1}^{j-1}(j-l)\sigma_l\right], \tag{B7}$$

which is Eq. 11) for $u_j=u_j^s$.

To find $v_j(t)=u_j(t)-u_j^s$, we note that it satisfies Equation (9) with zero RHS and insert in that equation the eigenvector expansion

$$v_j(t)=\sum_{n=1}^{N}V_{n,j}(t)\phi_{n,j}, \tag{B8}$$

$$-K_N^2\left(\phi_{n,j+1}+\phi_{n,j-1}-2\phi_{n,j}\right)=\Omega_n^2\phi_{n,j}, \tag{B9}$$

where eigenfrequencies Ω_n and eigenvectors $\phi_{n,j}$ are given by (13) and (14), respectively. Eq. (B9) can be checked by direct computation. The eigenvectors $\phi_{n,j}$ of the discrete Laplacian satisfy the orthogonality condition

$$\sum_{n=1}^{N}\phi_{n,j}\phi_{m,j}=\delta_{nm}, \tag{B10}$$

The result is

$$\ddot{V}_{n,j}+\Omega_n^2V_{n,j}=0, \tag{B11}$$

thereby producing $V_{n,j}=A_n\cos(\Omega_n t)+B_n\sin(\Omega_n t)$ which, inserted in (B8), yields Eq. (12). Equation (13) of the main text, giving A_n and B_n, follows from the initial conditions for $u_j(t)$ and the orthogonality condition (B10) for the eigenvectors $\phi_{n,j}$.

[1] J. Kanamori, J. Appl. Phys. **31**, S14 (1960); E. Pytte Phys. Rev. B **8**, 3954 (1973); J. Feder, E. Pytte Phys. Rev. B **8**, 3978 (1973); P. A. Rikvold, Z. Phys. B **26**, 195 (1977).

[2] T. Schneider, E. P. Stoll, Phys. Rev. Lett. **31**, 1254 (1973) and Phys. Rev. B **17** 1302 (1977); P. A. Rikvold, Bussei Kenkyu **33** (5), E43 (1980).

[3] F.J. Pérez-Reche, L. Truskinovsky and G. Zanzotto, Phys. Rev. Lett. **99**, 075501 (2007) and Phys. Rev. Lett. **101**, 230601 (2009).

[4] R.J. Glauber, J. Math. Phys. **4**, 294 (1963).

[5] A. Prados, L.L. Bonilla, A. Carpio, J. Stat. Mech. P06016 (2010); L.L. Bonilla, A. Prados, A. Carpio, J. Stat. Mech. P09019 (2010).

[6] J. C. Meyer, A. K. Geim, M.I. Katsnelson, K. S. Novoselov, T. J. Booth, S. Roth, Nature **446** 60 (2007).

[7] J. C. Meyer, C. Kisielowski, R. Erni, M.D. Rossell, M.F. Crommie, A. Zettl, Nano Lett. **8**, 3582 (2008).

[8] A. Carpio, L.L. Bonilla, Phys. Rev. B **78**, 085406 (2008); A. Carpio, L.L. Bonilla, F. de Juan, M.A.H. Vozmediano, New J. Phys. **10**, 053021 (2008); L.L. Bonilla, A. Carpio, Continuum Mech. Thermodyn. **23**, 337 (2011).

[9] L.L. Bonilla and A. Carpio, p. 167 in *Graphene Simulation*, edited by Jian Ru Gong. Intech, 2011. ISBN: 978-953-307-556-3.

[10] In the continuum limit, the equation of motion, $\ddot{u}_j-\omega^2(u_{j+1}+u_{j-1}-2u_j)=f\sigma_j/m$ becomes the wave equation $\partial^2u/\partial t^2-c^2\partial^2u/\partial x^2=f\sigma/m$, with $u_j(t)=u(x,t)$ and $c=\omega\chi$, provided $x=\chi j=jL/N$ is finite as j and N go to infinity and L is the string length. A finite wave velocity implies that $\omega\propto N$. Different scalings of the parameters may produce the same result of

a size-independent critical temperature. For instance, a finite T_c is also obtained for $\omega \propto N$, $m \propto 1/N$ and $f \propto 1/\sqrt{N}$. In both cases we find a finite wave velocity $c = \omega L/N \sim \omega L/(\pi K_N) = \omega_0 L/\pi$ in the continuum limit.

[11] J. Atalaya, A. Isacsson, J. M. Kinaret, Nano Letters **8**, 4196 (2008).

[12] A. H. Castro-Neto, F. Guinea, N. M. R. Peres, K. S. Novoselov, A. K. Geim, Rev. Mod. Phys. **81**, 109 (2009).

[13] J. H. Los, M. I. Katsnelson, O. V. Yazyev, K. V. Zakharchenko, A. Fasolino, Phys. Rev. B **80**, 121405(R) (2009).

[14] P. San-Jose, J. González, F. Guinea, Phys. Rev. Lett. **106**, 045502 (2011).

[15] S. Viola Kusminskiy, D. K. Campbell, A. H. Castro-Neto, F. Guinea, Phys. Rev. B **83**, 165405 (2011).

[16] A.Eichler, J. Moser, J.Chaste, M. Zdrojek, I. Wilson-Rae, A. Bachtold, Nature Nanotechnology **6**, 339 (2011).

[17] See Supplemental Material at [URL will be inserted by publisher] for movies showing the time evolution of the string, corresponding to the different physical situations depicted in figures 1 and 2.